DESIGN OF CODED APERTURE OPTICAL ELEMENTS FOR SUPERKEKB X-RAY BEAM SIZE MONITORS

E. Mulyani, Sokendai, Tsukuba, Ibaraki, Japan
J.W. Flanagan, KEK and Sokendai, Tsukuba, Ibaraki, Japan

Abstract

We describe the design of coded aperture optical elements for the SuperKEKB x-ray beam size monitors. X-ray beam profile monitor are being installed in each ring of SuperKEKB (LER and HER) to provide high resolution bunch-by-bunch, turn-by-turn measurement capability for low emittance tuning, collision tuning and instability measurements[1,2]. We use two types of optical elements, single-slit (pinhole) and multi-slit optical elements (coded apertures, CA). CA imaging offers greater open aperture than a single pinhole, for greater photon throughput and better statistical resolution for single-shot measurements. X-rays produced by a hard-bend magnet pass through a pinhole or CA optical element onto a detector. The resolution is obtained by calculating the differences between the images recorded by the detector for various simulated beam sizes, for a given number of photons. The CA elements that we have designed for use at SuperKEKB are estimated to provide 1.25-2.25 microns resolution for 10-25 microns of vertical beam sizes at 1 mA bunches. We present the design principle and optimizing process used to optimize the resolution at various beam sizes for SuperKEKB.

INTRODUCTION

Precision measurement of vertical bunch size plays an important role in the operation and tuning of electron storage rings [3], including the e^+ e^- collider SuperKEKB[4]. For this machine, luminosity or brightness is directly related with vertical emittance and vertical beam size. To meet bunch-by-bunch beam profile monitoring with high resolution and fast response, we are building an x-ray imaging system based on coded aperture (CA) imaging [5]. The basic concept of CA imaging is shown in Fig. 1. The system consists of a pseudorandom array of pinholes (apertures) that project a mosaic of pinhole images onto a detector. The detector image is then decoded using the known mask pattern to reconstruct the original image. With a single pinhole, the resulting image is relatively easy to understand and analyze, though the usable photon flux is limited.

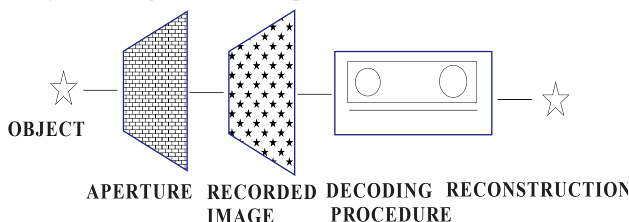

Figure 1: Basic concept of CA imaging [6].

CA imaging offers greater open aperture than a single pinhole, for greater photon throughput and better statistical resolution for single-shot measurements. One traditional example of such a pattern is the Uniformly Redundant Array (URA)[6], which has been tested for beam size measurement at CesrTA[7], Diamond Light Source[8], and the ATF2[9]. Other patterns have also been developed which are optimized for better performance at small beam sizes [10]. At SuperKEKB, x-ray beam monitors will be used primarily for vertical bunch profile measurement, with two types of optical elements, single-slit (pinhole) and multi-slit optical elements (coded apertures, CA). A schematic view of the x-ray beam size monitor line is shown in Fig. 2. Beryllium filters are placed upstream of the optics to reduce heat load, with the whole line being in vacuum up to the 200 µm Be extraction windows at the end. The detector is 128 channels of silicon with 2 mm of sensing depth, and a pixel pitch of 50 µm. SuperKEKB has two rings, the Low Energy Ring (LER) and the High Energy Ring (HER). Parameters for each beam line and the optical elements shown in Table 1.

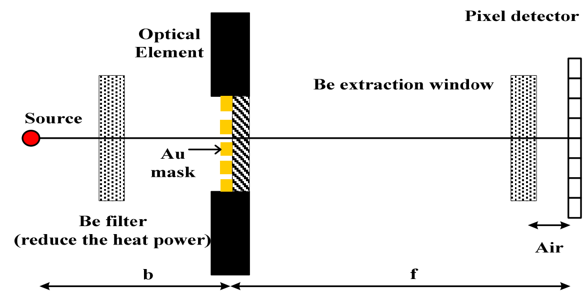

Figure 2: Simplified schematic of x-ray beam size Table monitor (not to scale).

Table 1: Parameter for Beam Lines and Optical Element

Parameter	LER	HER	Unit
Beam energy	4	7	GeV
Source bend radius ρ	31.74	106	m
Distance from source to mask (b)	9.43	10.33	m
Distance from mask to detector (f)	31.38	32.35	m
Au thickness	20	20	µm
Total Be thickness (filter+window)	0.7	16.2	mm
Diamond thickness	600	600	µm
Air gap (window-det.)	10	10	cm

Copyright © 2015 CC-BY-3.0 and by the respective authors

ISBN 978-3-95450-176-2

SIMULATION METHODS

The formalism used to simulate the detected image follows K.J.Kim's formulation [11, 12]

$$\begin{pmatrix} A_\sigma \\ A_\pi \end{pmatrix} = \frac{\sqrt{3}}{2\pi}\gamma\frac{\omega}{\omega_c}\left(1+X^2\right)(-i)\begin{pmatrix} K_{2/3}(\eta) \\ \frac{iX}{\sqrt{1+X^2}}K_{1/3}(\eta) \end{pmatrix} \quad (1)$$

where

$$\begin{aligned} \eta &= \frac{1}{2}\frac{\omega}{\omega_c}\left(1+X^2\right)^{3/2} \\ X &= \gamma\psi \\ \omega_c &= 3\gamma^3 c/2\rho \end{aligned} \quad (2)$$

where $A_{\sigma,\pi}$ are the components of the complex wavefront amplitude of the synchrotron radiation (SR) with angular frequency of photon ω, γ is the Lorentz factor for the particle beam, ω_c is the critical frequency, ρ is the radius of instantaneous curvature of the electron trajectory (in practical units $\rho[m] = 3.3E[GeV]/B[T]$), ψ is the observation angle in the vertical plane and K are the modified Bessel functions. The angular density of the spectral flux in frequency band $\Delta\omega/\omega$ is defined as[11]

$$\begin{bmatrix} \frac{d^2F_\sigma}{d\theta d\psi} \\ \frac{d^2F_\pi}{d\theta d\psi} \end{bmatrix} = \alpha\frac{\Delta\omega}{\omega}\frac{I}{e}\left|\begin{matrix} A_\sigma \\ A_\pi \end{matrix}\right|^2 \quad (3)$$

where $d\theta$ is the horizontal angel element, α is the fine-structure constant, I is the accelerator beam current and e is the charge of the electron. As has been explained previously[13], for a one dimensional mask, the path integral in the vertical direction from a point in the source distribution to a point on the detector can be written using the Kirchhoff approximation as[14]

$$\begin{aligned} A_{\sigma,\pi}(\text{detector}) &= \frac{iA_{\sigma,\pi}(\text{source})}{\lambda} \\ &\times \int_{mask}\frac{t(y_m)}{r_1 r_2}e^{i\frac{2\pi}{\lambda}(r_1+r_2)}\left(\frac{\cos\theta_1+\cos\theta_2}{2}\right)dy_m \end{aligned} \quad (4)$$

where λ is the wavelength, y_d and y_m are the vertical coordinates at the detector and mask, r_1 and θ_1 are the distance and angle from the source point to the mask point at y_m, and r_2, θ_2 are the distance and angle from the mask point y_m to the detector point y_d. For each pixel in the detector, the wavefront amplitude from each source point is calculated by equation (4) and converted to detected flux.

The single-shot resolution of the system is limited by the statistical fluctuations in the number of detected photons. To estimate the resolution of the system as a function of beam size, simulated images are calculated for Gaussian beams of various sizes. The simulated detector images for different-sized beams are then compared pair-wise against each other. The differences between two images in signal height for each channel are used to calculate the χ^2 per degree of freedom as[15]

$$\frac{\chi^2}{\nu} = \frac{1}{N-n-1}\sum_{i=1}^{N}\frac{\left[s_i' - s_i\right]}{\sigma_i^2} \quad (5)$$

where N is the number of detector channels (pixels), and n is the number of fit parameters, which is in this case is one. The residual weighting σ_i for channel is taken to be proportional to the square root of the signal height (number of photons) in that channel (s_i). The resolution is then defined as the change in beam size, Δσ, where the χ^2 per degree of freedom is one.

MASK DESIGN

The optical elements for the x-ray beam size monitor consist of 20 µm thick gold masking material on 600 µm thick diamond substrates. The diamond substrate mask is more robust than silicon (due to the better heat conduction of diamond), so it can better tolerate the LER and HER power densities [16]. The design of the pinhole and CA masks proceeded as follows. First, the pinhole size was optimized by simulating detector images for a point source in both rings, with various pinhole (slit) sizes. The minimum widths of the resulting Point Response Functions (PRFs) were found to be the same (within 1 µm) at 33 µm for both the LER and the HER, so this size pinhole was taken as the optimum for both rings. Next, pairs of 33 µm slits were simulated, with varying separations between the pairs.

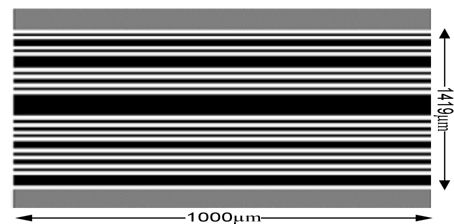

Figure 3: CA1 mask with 17 slits.

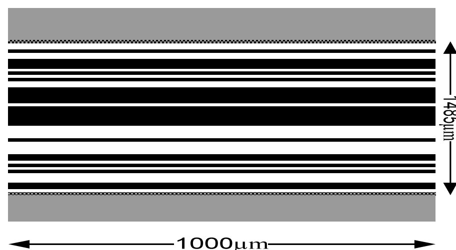

Figure 4: CA2 mask with 12 slits.

Copyright © 2015 CC-BY-3.0 and by the respective authors

ISBN 978-3-95450-176-2

For each separation, the resolution curves for different beam sizes at a standard bunch current of 1 mA were calculated, to determine the range of beam sizes for which each slit separation was optimal. Then a series of multi-slit patterns were devised by hand, incorporating a suitable range of slit separations to cover the dynamic range of interest, with emphasis on covering the smallest beam sizes. The hand-optimized pattern that was chosen based on its resolution curve over a range of beam sizes is denoted CA1, shown in Fig. 3. Finally, a 12-slit URA pattern was constructed using 33 µm as the basic unit size. This pattern, called CA2, is shown in Fig. 4.

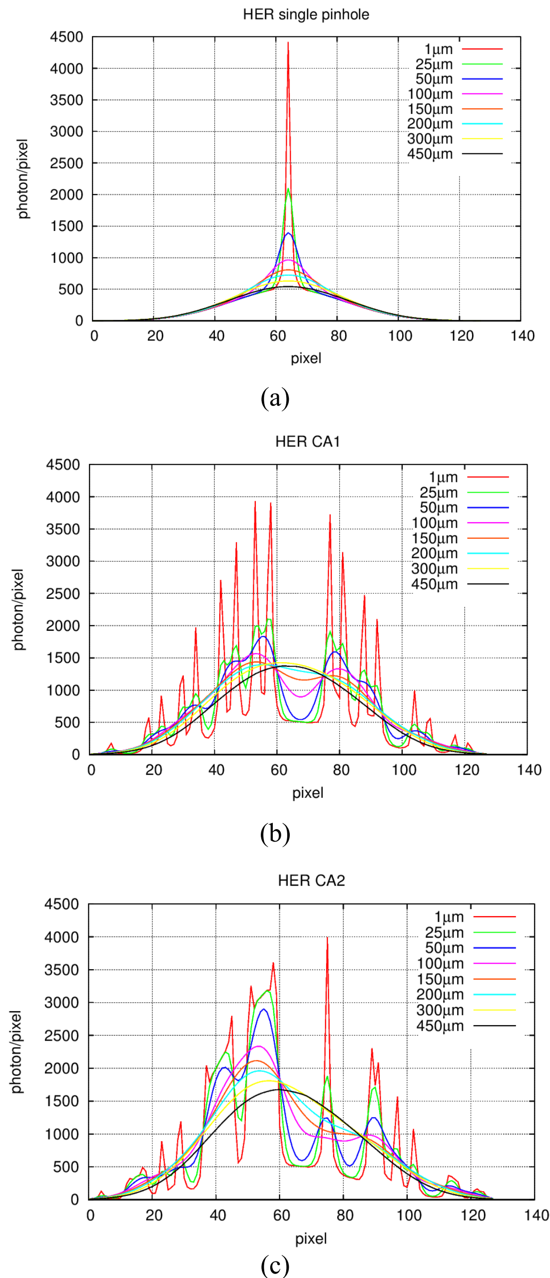

Figure 5: Simulated detector images showing the number of photons/pixel for 1 mA bunches for different beam sizes at HER: (a) single pinhole; (b) CA1; (c) CA2.

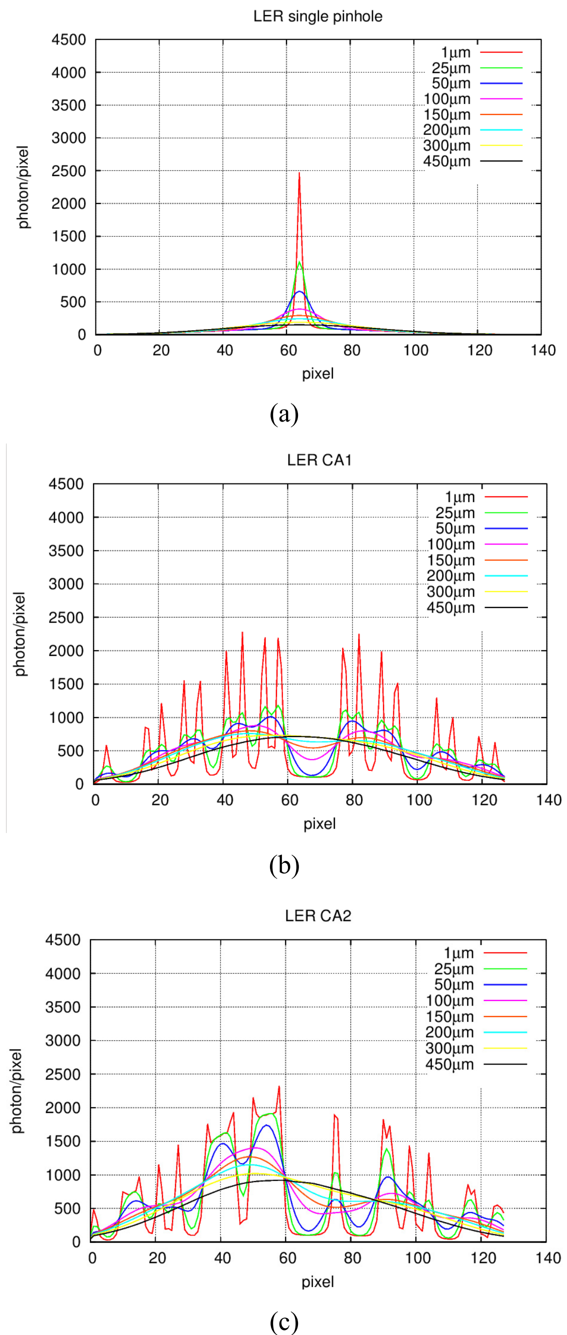

Figure 6: Simulated detector images showing the number of photons/pixel for 1 mA bunches for different beam sizes at LER: (a) single pinhole; (b) CA1; (c) CA2.

RESULTS

The detector images for all three optical elements at the HER and LER are shown in Figs. 5 and 6, respectively.

We calculated the resolutions for the pinhole and the CA masks for both rings (LER and HER) with the number of photons in the LER being 1942.96 photon/turn/mA/bunch, while at the HER it is 3341.63 photon/turn/mA/bunch, for hole regions. Figs. 7 and 8 show the estimated resolution for the single-slit, CA1 and CA2 for various bunch currents.

ISBN 978-3-95450-176-2

Copyright © 2015 CC-BY-3.0 and by the respective authors

At lower beam sizes (10-25 microns), the CA1 has better single-shot resolution than the single pinhole and CA2. It is estimated to provide 1.25-2.25 microns resolution for 10-25 microns of vertical beam sizes at 1 mA bunches. For smaller currents the resolution of vertical beam sizes changes, e.g at 0.1 mA and 0.01 mA bunches the resolution drops to 4-7.5 microns and >20 microns respectively due to lower photon throughput and statistical resolution. For higher beam sizes (> 30 μm), the CA2 mask performs better than CA1.

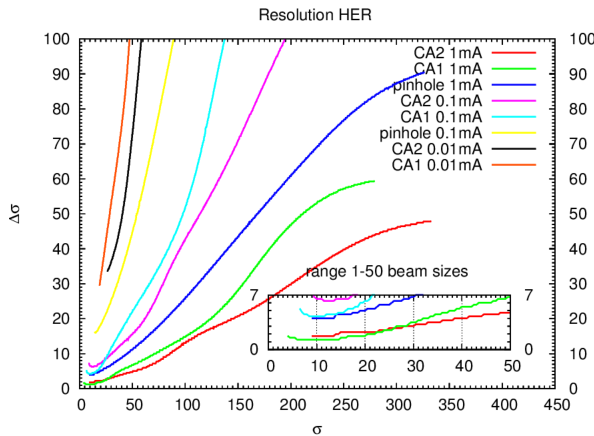

Figure 7: Vertical beam size resolutions at HER for various bunch currents (1 mA, 0.1 mA and 0.01 mA) and optical elements (single pinhole, CA1 and CA2).

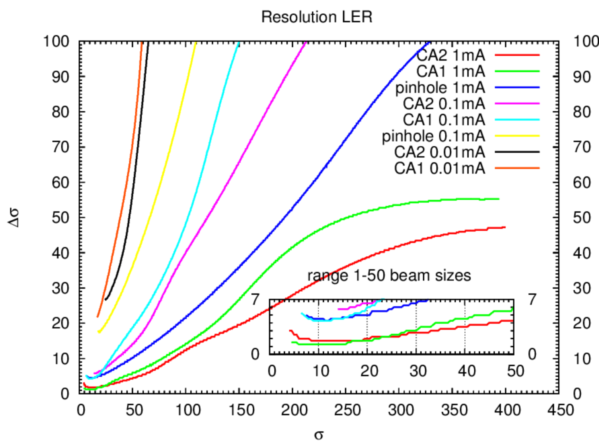

Figure 8: Vertical beam size resolutions at LER for various bunch currents (1 mA, 0.1 mA and 0.01 mA) and optical elements (single pinhole, CA1 and CA2).

SUMMARY

The CA1 elements that we have designed for use at SuperKEKB are estimated to provide 1.25-2.25 microns resolution for 10-25 microns of vertical beam sizes at 1 mA bunches. For larger beam sizes (> 30 μm), CA2 mask is better than CA1.

The pinhole and CA masks are in fabrication for use at SuperKEKB. The study of the resolutions available with these mask patterns will be refined to incorporate noise and low-count (Poisson) statistics, and compared with data taken following beam commissioning in Spring 2016.

REFERENCES

[1] H. Fukuma, et al., Proc. IBIC2013, 6 (2014).
[2] J.W. Flanagan, et al., Proc. PASJ10, Himeji, (2010).
[3] J.W. Flanagan, Proc. IPAC11, 1959 (2011).
[4] Z. Dolezal, for the Belle Collaboration, PoS EPS-HEP2009, p. 143 (2009).
[5] R. H. Dicke, Astrophys. Journ., 153, L101 (1968).
[6] E. E. Fenimore, T. M. Cannon, Appl. Optics, Vol 17, No.3, 337 (1978).
[7] J.P. Alexander et al, Nucl. Instrum. Methods Phys. Res., Sect. A **748**, 96 (2014).
[8] C. Bloomer, et al., Proc. IBIC2014, TUCBZ2 (2014).
[9] J.W. Flanagan, et al., Proc. IBIC2012, 237 (2012).
[10] J.P. Alexander et al, Nucl. Instrum. Methods Phys. Res., Sect. A **767**, 467 (2014).
[11] K. J. Kim, AIP Conf. Proc. **184**, 565 (1989).
[12] A.Thompson et al., X-ray Data Booklet, (Berkeley : Lawrence Berkeley National Laboratory, 2009), 2-1.
[13] J.W. Flanagan et al., Performance of Coded Aperture X-Ray Optics with Low Emittance Beam at CESRTA, Proc. PAC09, Vancouver, BC, Canada, pp. 3561-3563 (2009).
[14] J.D. Jackson., *Classical Electrodynamics*, (Second Edition), John Wiley&Sons, New York (1975).
[15] P.R. Bevington, *Data Reduction and Error Analysis for the Physical Sciences*, McGraw-Hill, New York (1969).
[16] J.W. Flanagan et al., Proc. IBIC2013, 844 (2013).

Copyright © 2015 CC-BY-3.0 and by the respective authors

ISBN 978-3-95450-176-2